Quaternary Science Reviews
September 2015, Volume 123 Pages 134-143
https://doi.org/10.1016/j.quascirev.2015.06.007
https://archimer.ifremer.fr/doc/00504/61601/

Changes in the strength of the Nordic Seas Overflows over the past 3000 years

Moffa-Sanchez Paola [1, *], Hall Ian R. [1], Thornalley David J. R. [2, 3], Barker Stephen [1], Stewart Connor [1]

[1] Cardiff Univ, Sch Earth & Ocean Sci, Cardiff CF10 3AT, S Glam, Wales.
[2] UCL, Dept Geog, London WC1E 6BT, England.
[3] Woods Hole Oceanog Inst, Dept Geol & Geophys, Woods Hole, MA 02543 USA.

* Corresponding author : Paola Moffa-Sanchez, email address : paolamoffa@marine.rutgers.edu

Abstract :

The Nordic Seas Overflows constitute the densest component of the deep limb of the Atlantic Meridional Overturning Circulation (AMOC). Changes in the vigour of the overflows may have had important climatic effects in the past and may also have in the future. Yet, evidence for multidecadal to millennial changes in the deep limb of the AMOC and their potential relationship to North Atlantic climate variability during the Holocene remains weakly constrained. Here we present grain size data, as a proxy for near-bottom current speed, from sub-decadal to decadally resolved sediment cores located in the direct pathway of the two Nordic Overflows east and west of Iceland, the Iceland-Scotland Overflow Water (ISOW) and the Denmark Strait Overflow Water (DSOW), respectively. The results show no clear relationship between reconstructed changes in the vigour of the Nordic Overflows and the well-known periods of centennial-scale climate variability recorded in the North Atlantic region. However, well-defined millennial-scale trends are found in both of the overflow strength records over the last 3000 years, which were possibly related to hydrographic reorganizations in the Nordic Seas, driven by the decrease in Northern Hemisphere summer insolation over the Neoglacial period. A comparison between the near-bottom flow speed reconstructions from ISOW and DSOW suggests an anti-phased relationship between the Nordic Seas Overflows east and west of Iceland over the last 3000 years. This feature has been observed in climate models potentially as a result of shifts in the deep water formation sites as a response to changes in atmospheric patterns over the Nordic Seas.

Highlights

► Sortable silt records show variability in the strength of the Nordic Seas Overflows over the last 3000 years. ► Changes in the overflows vigour likely resulted from Neoglacial surface hydrography reorganisation in the Nordic Seas. ► The strength of two overflows east and west of Iceland appear antiphased for the last 3000 years.

Keywords : Late Holocene, North Atlantic, Nordic Overflows, Paleoceanography

1. Introduction

The warm salty surface waters, originating in the tropics, are transported to the higher latitudes across the North Atlantic reaching the Nordic Seas and Arctic Ocean. During their northward transit these inflowing Atlantic waters lose heat to the atmosphere, via air-sea exchange, increase their density and eventually sink to form intermediate and deep water masses, via convective processes, in the Nordic Seas. This process is often referred as the Atlantic Meridional Overturning Circulation (AMOC) and since it regulates the transport and distribution of heat, nutrients and CO_2 around the Earth's oceans, changes in the strength and structure of it have often been thought to be involved in past climate variability, particularly in the North Atlantic region [e.g. *Kuhlbrodt et al.*, 2007].

The submarine ridge that lies between Greenland and Scotland, the Greenland-Scotland Ridge (GSR), forms a physical barrier that controls the exchange of deep dense waters between the Nordic Seas and the North Atlantic [e.g. *Meincke*, 1983] (Figure 1). The dense waters that flow across the GSR into the North Atlantic Basin are collectively referred to as the Nordic Seas Overflows. These overflows are of pivotal importance to the climate system since they provide ~30% of the volume transport of the lower limb of the AMOC and downslope entrainment with intermediate waters when entering the Atlantic Basin, increases the volume transport of the deep waters by three fold [*Dickson and Brown*, 1994; *Hansen et al.*, 2004]. Furthermore, the overflow of deep waters into the North Atlantic also helps set the pressure gradient at the surface, which contributes significantly to the northward inflow of warm waters into the Nordic Seas [*Hansen et al.*, 2010]. The advection of heat and salt to the high latitudes via the Atlantic inflow is important not only for ameliorating the climate in Western Europe [*Rossby*, 1996] but also for promoting deep water formation. Additionally, modelling studies have suggested that the density of the overflows and their transport can

65 also influence the surface hydrography south of the GSR, namely the subpolar gyre
66 circulation [*Born et al.*, 2009; *Zhang et al.*, 2011].
67
68 Future climate simulations under increasing atmospheric CO_2 levels predict a change in the
69 freshwater budget in the Arctic Ocean and Nordic Seas as a result of a decline in Arctic sea
70 ice cover, melting of the Greenland Ice Sheet and increase in circum-Arctic river run-off
71 [*Stocker et al.*, 2013]. The addition of freshwater into the high latitudes may lower the surface
72 ocean salinity and reduce the formation of dense waters in the Nordic Seas, which would
73 potentially weaken the overflow transport across the ridge, possibly affecting the AMOC
74 [*Hansen et al.*, 2004; *Wilkenskjeld and Quadfasel*, 2005; *Rahmstorf et al.*, 2015].
75
76 However, prior to reaching any conclusion on the anthropogenic drivers of climate change
77 and their potential effect on the freshening and weakening of the overflows and the AMOC, it
78 is necessary to extend the instrumental records of overflow vigour back in time to improve
79 our understanding of the natural variability of these key components of the AMOC. On
80 centennial time-scales, proxy reconstructions have revealed abrupt changes in the strength
81 and/or depth of the overflow boundary currents at times corresponding to well-known
82 millennial-centennial scale climatic oscillations, such as the 8.2 kyr event [*Ellison et al.*,
83 2006], the 2.7 kyr event [*Hall et al.*, 2004] and the Little Ice Age [*Bianchi and McCave*,
84 1999], and over the Holocene [*Thornalley et al.*, 2013]. This ocean-climate link suggests that
85 the Nordic Sea Overflows, and their role in setting the strength of the AMOC, play a leading
86 role in modulating climate variability over the current interglacial.
87
88 Here we present near-bottom flow speed reconstructions from two sub-decadal to decadally
89 resolved marine sediment cores which are strategically located within the present day flow

path of the two main Nordic Sea Overflows, namely Iceland Scotland Overflow Water (ISOW) and Denmark Strait Overlow Water (DSOW) respectively, and which span the last 3000-4000 years. In order to reconstruct the relative flow speed changes we use the paleocurrent proxy 'sortable silt' mean grain size ($\overline{SS}$), which is the average of the 10–63 μm terrigenous fraction [*McCave et al.*, 1995]. Size sorting in this size range responds to hydrodynamic processes and can therefore be used to infer relative changes in the speed of the depositing current [*McCave et al.*, 1995; *McCave and Hall*, 2006].

2. Hydrographic Setting: The Nordic Overflows

Deep water formation in the Nordic Seas sets a horizontal density gradient across the GSR which drives the transfer of these dense waters over the sill as the Nordic Sea Overflows [*Hansen et al.*, 2001]. The rate of dense water export by the overflows into the North Atlantic Basin is hydraulically controlled and is proportional to the cross-sill density difference of the water masses and to the upstream reservoir height [*Whitehead*, 1998]. Alteration of these factors drives changes in the vigour of the overflows reaching the Atlantic Basin.

The densest overflow waters pass through the deepest passages of the GSR, the Denmark Strait and the Faroe Bank Channel. As such, the Nordic Sea Overflows are divided into two major branches east and west of Iceland: the Iceland Scotland Overflow Water (ISOW) and the Denmark Strait Overflow Water (DSOW), respectively (Figure 1). While the two overflows are different primarily because of the differing sill geometries and the physical properties of their upstream source waters, both overflows contribute ~3 Sv each (1 Sv = 10^6 m^3 s^{-1}) to the total volume flux of dense waters ventilating the deep subpolar North Atlantic [*Olsen et al.*, 2008 and references therein]. Once the overflows cross the GSR, they descend over the sill subsequently entraining intermediate waters found in the Irminger and Iceland

Basins, such as Labrador Sea Water and other Subpolar Mode Waters. Thereafter, the overflows continue as density-driven bottom currents, following the bathymetry whilst undergoing further mixing with the overlying waters. This intensive downstream entrainment and mixing increase the initial volume transport by three-fold and significantly alter the hydrographic properties of the overflow waters [*Price and Baringer*, 1994]. The two overflows (ISOW and DSOW) merge south of the Denmark Strait forming the upper and lower branches of the Deep Western Boundary Current (DWBC) on reaching Cape Farewell, although here the different water masses are still distinguishable based on potential density [*Holliday et al.*, 2009]. The DWBC subsequently flows around the Labrador Basin (Figure 1) and in combination with Labrador Sea Water (LSW) eventually forms North Atlantic Deep Water (NADW), which constitutes the deep limb of the AMOC.

3. Materials

3.1. **Core settings**

Sediment core RAPiD-17-5P (61° 28.90'N, 19° 32.16'W, 2303 m water depth) is situated on the deeper section of the south Iceland insular rise that runs along the northern edge of the South Iceland Basin (Figure 1) [*Thornalley et al.*, 2010]. Numerous hydrographic and hydro-chemical studies focusing on the deep circulation in the Iceland Basin [*Van Aken*, 1995; *van Aken and Becker*, 1996; *Bianchi and McCave*, 2000; *Fogelqvist et al.*, 2003] and the Conductivity Temperature Depth (CTD) data obtained during the CD159 cruise [*McCave*, 2004] show bottom temperatures and salinities of ~2.8-3°C and ~34.97 respectively at the core site, which confirm that RAPiD-17-5P lies directly in the present day pathway of the ISOW.

Sediment core RAPiD-35-COM is a composite record comprising box-core RAPiD-35-25B [*Moffa-Sanchez et al.*, 2014b] and the piston core RAPiD-35-14P (57° 30.25'N, 48° 43.34'W, 3484 m water depth) both recovered from the same site located on the Eirik Ridge, south east of the southern tip of Greenland. CTD transects on the Eirik Ridge, show a temperature of <2^{o}C and salinity of 34.9 at the core location (3500 m water depth) [*Holliday et al.*, 2009]. CTD measurements obtained during the CD159 cruise at two neighboring locations (58° 14N, 47° 00W and 56° 45N, 52° 27W) in the Labrador Basin show temperatures and salinities of 1.6-1.75 ^{o}C and 34.86-34.89 respectively (>3000 water depth) [*McCave*, 2004]. Both lines of evidence indicate that the core location currently lies in the pathway of the DSOW (defined as >27.88 kg/m^3) (Hunter et al., 2007a).

3.2. Core-chronology

The core-chronology for RAPiD-17-5P has been previously published in Moffa-Sánchez et al. [2014a] and it is presented in the Supplementary Material of this article. The age model for RAPiD-17-5P was constructed based on a linear fit through the twelve radiocarbon dates, implying a constant sedimentation rate of approximately 80 cm/kyr for the last 9000 years (R^2=0.99) [*Moffa-Sanchez et al.*, 2014a]. The good linear fit to the calibrated dates suggests a probable lack of abrupt changes in the rate of the sediment deposition during the time interval studied. The core was sampled at 0.5 cm intervals and thus each data point represents an integrated time of ~6 years. The core-top of RAPiD-17-5P was lost as the piston core over penetrated [*McCave*, 2004]; the top 1 cm has a calibrated age of ~1737 years AD.

The age-model for RAPiD-35-14P (57°30.25', 48°43.34', 3484 m) was constructed using ten ^{14}C AMS dates measured from monospecific samples of the planktonic foraminifer *Neogloboquadrina pachyderma (sinistral)* (>150 μm) and were converted to calendar years

using MarineCal13 dataset [*Reimer et al.*, 2013]. The core-chronology was constructed using a Bayesian Age-Model software; BChron [*Haslett and Parnell*, 2008; *Parnell et al.*, 2011] (Table 1, Figure 2). Based on the ^{14}C dating and further validated by the coarse fraction percent in the two cores, the splicing point between the bottom of the box-core RAPiD-35-25B [*Moffa-Sanchez et al.*, 2014b] and the piston core RAPiD-35-14P, was assigned to a depth of 30 cm in RAPiD-35-14P (Figure 2). This spliced record is referred to as RAPiD-35-COM hereinafter.

4. Methodology

4.1. Sortable Silt

Sortable silt mean grain size ($\overline{SS}$) is defined as the mean grain size of the 10- 63 μm terrigenous material [*McCave et al.*, 1995]. The particles in this size range behave non-cohesively (i.e. without adhering to one another) and are therefore sorted by primary particle size in response to hydrodynamic processes. Consequently, $\overline{SS}$ can be used to infer relative changes in the near-bottom speeds of its depositing current [*McCave et al.*, 1995; *McCave and Hall*, 2006].

The sediment for $\overline{SS}$ analysis was prepared following the method outlined by McCave et al. [1995]. This involves the removal of carbonate and biogenic opal using 2M acetic acid and 2M sodium carbonate at 85 ^{o}C for 5 hours. The acid step was repeated twice (each batch of acid was left in the samples for at least 24 hours) it was followed by a water rinse before the addition of sodium carbonate to the sample. The samples in sodium carbonate were then placed in the water bath for 5 hours at 85 ^{o}C and vigourous stirring was carried out 3 times during this time interval to promote dissolution of the biogenic silica. Once the carbonate and biogenic opal removal steps were completed the samples were suspended in 0.2 %

190 sodium hexametaphosphate (Calgon) dispersant in 60 ml Nalgene bottles. To ensure full
191 disaggregation, all samples were placed on a rotating wheel for a minimum of 24 hours and
192 were finally ultrasonicated for 3 minutes immediately prior to the sample analysis using a
193 *Beckman Multisizer 3 Coulter Counter*. For each run, two aliquots of the same sample (150
194 µl) were pipetted into the beaker as a measure to minimise the procedural error attached to
195 pipetting.
196
197 As detailed in Bianchi et al. [1999], the Coulter Counter aperture size was set for 140 µm. A
198 particle sizing and counting threshold was set to 8 µm and 10 µm respectively, with a sizing
199 bin of 256 and the total count of 70,000 particles in the 10-63 µm size range was performed
200 for each run. The samples were run with a suspended particle concentration of <4%
201 (generally between 1- 2.5%). Initial analysis showed poor precision (up to 3 µm), which was
202 caused by the settling of the particles from the sample in suspension over the period of the
203 analyses. This was overcome by elevating the speed of the stirrer (speed 54). Additionally,
204 the volume of electrolyte (Isoton^{TM}) used to suspend the sample was increased in order to
205 avoid turbulence and drawdown of bubbles into the sample at the higher stirrer speed. The
206 sample blank under the higher stirrer speed did not produce significant background noise.
207 Each sample was run a minimum of twice in an arbitrary order and over several days. The
208 average standard deviation from the duplicate or triplicate runs was ±0.6 and ±0.1 µm in
209 RAPiD-17-5P and RAPiD-35-COM, respectively.

210 **4.2. Statistical and Spectral Analysis**

211 Single Spectral analysis was performed using a multi-taper method [*Pardoiguzquiza et al.*,
212 1994], and spectral confidence levels were located using the robust AR(1) modelling of
213 median-smoothed spectra [*Mann and Lees*, 1996]. Wavelet analysis was performed using
214 *Wavelet* from Torrence and Compo [1998] and in order to study the presence and timing

periodicities obtained in the single spectral analysis. Time-series correlation was performed using the PearsonT programme [*Mudelsee*, 2003]. In PearsonT, the Pearson's correlation coefficient is estimated employing a nonparametric stationary bootstrap confidence interval with an average block length proportional to the maximum estimated persistence time of the data [*Mudelsee*, 2003].

5. Results

5.1. RAPiD-17-5P (Iceland Basin)

The sub-decadal $\overline{SS}$ near-bottom flow speed reconstruction for ISOW in the Iceland Basin from RAPiD-17-5P shows a particle size variability of 6-8 μm for the last 3000 years (Figure 3e). The $\overline{SS}$ record shows the highest variability on a decadal timescale between 3000-2200 years BP with a broad well-defined minimum in $\overline{SS}$ occurring between 1850-1500 years BP with a low centered at 1750 years BP followed by a gradual steady decrease of ~4.5 μm since ~1500 years BP. Other marked slowdowns of ISOW occur at around 2250, 2050, 1250 and 950 yrs BP (Figure 3e).

Single spectrum and wavelet analyses were performed on the 18.6 yr (minimum time-step) gaussian interpolated $\overline{SS}$ records with a 56.9-yr window for RAPiD-17-5P. Cyclicities are found at 165 and 75 years at >95% and >90% Confidence Limit (CL), although wavelet analysis reveals that these cyclicities are not stationary throughout the record suggesting they are not a pervasive feature of the flow speed record (Supplementary Figure 1,2).

5.2. RAPiD-35-COM (Eirik Drift)

The near-bottom flow speed reconstruction for DSOW from RAPiD-35-COM (Eirik Drift) shows a $\overline{SS}$ variability of ~7 μm, ranging in grain sizes between 19-26 μm over the last 4000 years (Figure 4a). The record shows persistent low $\overline{SS}$ and relatively stable (decrease amplitude variability) between 2300-4000 years BP. At 2300 years BP the record shows a

shift to higher amplitude variability (Figure 4a inset) with also faster flow speeds becoming more prevalent towards the present. Additional centennial-scale lows in $\overline{SS}$ are found at 1900-2100, 1100-1500 and 300-500 years BP (Figure 4a).

Single spectrum and wavelet analysis on the 45-year Gaussian smoothed $\overline{SS}$ record from RAPiD-35-COM reveal some periodicities at around 500 years, 280 years and 180 years, with a hint of cyclicities at around 1500 years BP, however these cyclicities are not pervasive through the last 4000 years (Supplementary Figure 3,4).

6. Discussion

6.1. Multidecadal to centennial changes in the ISOW strength over the last 3000 years

The $\overline{SS}$ record from RAPiD-17-5P shows very defined and clear centennial to multidecadal oscillations (Figure 3e), however, it does not reveal a systematic relationship with previous reconstructions of climate variability derived from other sites within the North Atlantic, originally established from glacier advances and retreats by Denton and Kárlen [1973] and then synthesized and reviewed by Mayewski [2004] (Figure 3).

We use spectral analysis results to assess the possible presence of internal modes of variability of the ISOW vigour. Similarly to the recent study by Lohmann et al. [2014], the periodicities found in the 75-year domain could be related to the so-called Atlantic Multidecadal Oscillation (AMO). The AMO is defined as the interannual variability of sea surface temperature in the North Atlantic between 0-70^{o}N and have been observed to oscillate with periodicities of 50-88 years [*Schlesinger and Ramankutty*, 1994]. Modelling studies have suggested that the AMO arises from internal variability in the strength of AMOC [*Delworth and Mann*, 2000; *Knight et al.*, 2005], mostly via northward salt transport

feedbacks that occur in the order of 50-60 years [*Vellinga and Wu*, 2004]. Vellinga and Wu [2004] propose that a strong AMOC, enhances the transport of heat and salt to the higher latitudes creating a cross-equatorial sea surface temperature gradient that drives a northward migration of the ITCZ which will eventually freshen the tropical Atlantic and this freshwater anomaly will travel northwards and slowdown the AMOC. According to modelling work this process takes approximately 50-60 years [*Vellinga and Wu*, 2004].

The potential for a relationship between the AMO and the ISOW strength suggested by the spectral characteristics has also been observed in other grain size reconstructions [*Lohmann et al.*, 2014]. If correct, this would be evidence of the link between the strength of the AMOC and the AMO or more specifically the relationship between the sea surface temperatures within the Nordic Seas and the strength of the ISOW (as suggested by last millennium model results; *Lohmann et al.* [2014]). Nevertheless, the interpretation of the multidecadal cyclicities found in the $\overline{SS}$ records from ISOW is difficult particularly as firstly the short length of the proxy reconstructions of the AMO [1600 and 1300 years AD, *Gray et al.*, 2004; *Mann et al.*, 2009, respectively] precludes a confident comparison with the ISOW vigour and also the interpolated time-step of the ISOW may lead to some aliasing at this frequency. Further detailed discussion is therefore not included in this paper.

6.2. Long-term changes in the upstream ISOW vigour over the last 3000 years

To interpret the reconstructed past changes in ISOW strength it is essential to understand what controls the vigour of ISOW transport over the GSR and how these factors may have varied in the past. To this end, the close location of RAPiD-17-5P to the Greenland-Scotland Ridge is advantageous, as it is more sensitive to the hydraulically controlled transport of ISOW entering the Atlantic Basin [*Thornalley et al.*, 2013] than other sites located further downstream such as Gardar Drift [*Bianchi and McCave*, 1999; *Ellison et al.*, 2006], which

290 could potentially be modulated by Labrador Sea Water production because of entrainment
291 and mixing processes [*Boessenkool et al.*, 2007].
292 Therefore, variability in the strength of the ISOW recorded in RAPiD-17-5P could have
293 resulted from changes in the density and the reservoir height of the ISOW source waters
294 upstream of the GSR. The deep waters constrained north of the GSR in the Nordic Seas are
295 mostly formed by winter cooling and densification of warm surface Atlantic inflow waters.
296 Specifically, Norwegian Sea Deep Waters (NDSW), which is thought to be the main source
297 waters for ISOW, comprises a mixture of intermediate waters formed in the Norwegian Sea
298 mostly as a consequence of the cooling and densification of the warm salty Atlantic inflow
299 waters and intermediate waters formed during the cyclonic-loop of the Atlantic inflow waters
300 around the Nordic Seas and the Arctic Ocean [*Mauritzen*, 1996; *Eldevik et al.*, 2009]. It is for
301 this reason that past changes in the surface hydrography in the Nordic Seas may have a part
302 in the strength of deep water formation.
303
304 The surface hydrography in the Nordic Seas broadly consists of the south flowing East
305 Greenland Current (EGC) in the west of the basin, which transports low-salinity Arctic
306 waters along the East Greenland margin and on the eastern side of the basin by warm salty
307 Atlantic inflow waters flow as they flow northwards as the Norwegian Atlantic Current
308 (NwAC) (Figure 1). It is therefore possible, that the formation of NSDW was limited by the
309 volume and/or properties of Atlantic inflow or by an increase in polar waters reaching the
310 deep water formation sites. For instance, an increase of polar versus Atlantic waters in the
311 Norwegian Seas would likely result in an excess of freshwater at the surface which would
312 stratify the upper water column hence potentially inhibiting convection and decrease NSDW
313 formation.
314

315 A number of Holocene surface proxy reconstructions of the NwAC (from the Norwegian
316 Sea- MD95-2011, Voring Plateau and the Barents Sea- PSh5159N) present discrepancies in
317 the long term trends for the last 3000 years [*Calvo et al.*, 2002; *Risebrobakken et al.*, 2003;
318 *Andersen et al.*, 2004; *Moros et al.*, 2004; *Andersson et al.*, 2010; *Risebrobakken et al.*,
319 2010], and most of these reconstructions lack the high-temporal resolution in the RAPiD-17-
320 5P record, making direct comparison difficult. However, a high-resolution planktonic
321 foraminiferal $\delta^{18}O$ record with good age-constraints from the NwAC [*Sejrup et al.*, 2011],
322 reveals a similar decrease in temperature from 1750 years BP to present (Figure 3b), with a
323 similar trend to the one found in the RAPiD-17-5P $\overline{SS}$ record (Figure 3e). Ample evidence
324 also suggests a Late Holocene trend towards a cold and sea ice laden EGC with an increase in
325 the influence of polar waters and drift ice reaching North of Iceland via the East Icelandic
326 Current (EIC), a branch of the EGC [*Andrews et al.*, 1997; *Jennings et al.*, 2002; *Moros et al.*,
327 2006; *Müller et al.*, 2012; *Werner et al.*, 2013] and therefore potentially flowing into the
328 Norwegian Sea (Figure 3c).
329
330 This millennial scale trend was probably associated with an ocean regime dominated by
331 enhanced Arctic sea-ice production associated with a decline in summer insolation at these
332 latitudes (Figure 3). The drift ice would have been transported into the Nordic Seas via the
333 EGC. A Neoglacial increase in Arctic sea-ice and freshwater in the Norwegian Seas via an
334 increase in the transport by the EGC and EIC, would have shoaled convection, decreasing the
335 formation of NSDW as suggested by modelling studies [*Renssen et al.*, 2005; *Thornalley et*
336 *al.*, 2013]. A reduction in NSDW formation would have driven a decrease in ISOW vigour as
337 shown in the RAPiD-17-5P $\overline{SS}$ near-bottom flow speed reconstruction from 1500 years BP
338 onwards (Figure 3e). These millennial-scale changes in ISOW from RAPiD-17-5P are in
339 broad agreement with lower temporal resolution reconstructions of ISOW vigour [*Kissel et*

al., 2013; *Thornalley et al.*, 2013]. However, in the higher temporal resolution of our record we find that the Neoglacial trend may not have been as linear as previously suggested and it was interrupted by centennial episodes of slower ISOW such as the period centered around 1750 years BP, which is also evident in the Kissel et al. [2013] record. This feature indicates that other processes, aside from a decrease in summer insolation (Figure 3a) may have also played a role in the centennial scale-variability of the ISOW strength including feedbacks either arising either from internal climate dynamics or external forcings. However, the ISOW slowdown centered around 1750 years BP is not clearly evident in other North Atlantic surface ocean records, possibly due to the lower temporal resolution of most marine archives. Yet, temperature records from the Greenland Ice Sheet Project 2 (GISP2) do record a temperature drop around this time [*Alley*, 2000; *Kobashi et al.*, 2011] (Figure 3d), tentatively suggesting a linkage between a slowdown of ISOW and cooling in Greenland.

6.3. Variability in the DSOW strength South of Greenland

6.3.1. Sortable Silt mean grain size variability recorded in the Eirik Drift

Similar to RAPiD-17-5P, the centennial shifts in RAPiD-35-COM do not show any clear relationship with temperature reconstructions from other sites around the North Atlantic across this interval [*Denton and Karlén*, 1973; *Mayewski*, 2004] (Figure 4). Although Figure 4a shows a broad tentative correspondence of slower/faster flow speeds of DSOW with well-known cold/warm intervals, this is not the case during the Little Ice Age.

6.3.2. Source waters supplying DSOW: East Greenland Current versus North Icelandic Jet

The DSOW is formed by a complex and varied mixture of water masses deriving from the Arctic, Nordic Seas, re-circulating Atlantic waters and other minor water masses [*Rudels et al.*, 2002; *Tanhua et al.*, 2005; *Kohl et al.*, 2007; *Dickson et al.*, 2008]. Consequently, the variability of DSOW vigour could arise from changes in the relative contribution of its source

365 waters and/or in the hydrographic properties of these. Over the last few decades many
366 hydrographic and tracer studies have investigated the composition of DSOW, yet, it remains
367 unclear which water masses are the primary contributors. Some studies have suggested that
368 the DSOW is exclusively supplied by the EGC, which comprises a mixture of re-circulating
369 Atlantic waters (Atlantic waters that have undergone transformation and densification via
370 heat loss in and around the Nordic Seas) and polar waters formed in the Arctic and/or in the
371 Greenland Sea [*Swift and Aagaard*, 1981; *Strass et al.*, 1993; *Mauritzen*, 1996; *Rudels et al.*,
372 2002; *Jeansson et al.*, 2008; *Eldevik et al.*, 2009]. Others have proposed that intermediate
373 waters formed in the Iceland Sea as a result of winter cooling are the dominant constituent of
374 DSOW [*Swift et al.*, 1980; *Jonsson*, 1999; *Jonsson and Valdimarsson*, 2004; *Vage et al.*,
375 2011]. These two contrasting suggestions have often been referred to as Atlantic and Polar
376 sources of DSOW [*Eldevik et al.*, 2009].
377
378 The $\overline{\text{SS}}$ record from RAPiD-35-COM presents a gradual trend towards higher near-bottom
379 flow speeds of DSOW from ~2300 years BP to present with increased variance (Figure 4a).
380 This trend, is consistent with previous low-resolution grain size and mineral composition
381 results from the southwest Greenland Rise also indicating changes in DSOW around this time
382 [*Fagel et al.*, 2004]. Surface proxy records based on Ice Rafted Debris (IRD) counts, benthic
383 foraminiferal assemblages and organic geochemistry along the East Greenland margin also
384 reveal a consistent picture, indicating a progressive increase in sea ice and colder EGC for the
385 last 3000-4000 years (Figure 4b,c) [*Andrews et al.*, 1997; *Jennings et al.*, 2002; *Andersen et*
386 *al.*, 2004; *Moros et al.*, 2006; *Müller et al.*, 2012; *Werner et al.*, 2013]. A gradual increase in
387 the southern influence of polar waters reaching North Iceland has also been suggested by an
388 increase in terrigenous allochtonous quartz transported by drift ice by the EIC [*Moros et al.*,
389 2006; *Andrews*, 2009] (Figure 4). The increase in the southward advection of polar waters,

suggests either a gradual eastern shift of the polar front across the Nordic Seas and/or an increase in the southward transport of polar waters within the EGC throughout the Late Holocene. A concomitant increase in the volume transport of the EGC and DSOW vigour (Figure 4a-c) would be in agreement with the concept of the EGC as a dominant water mass source of DSOW [*Rudels et al.*, 2002; *Våge et al.*, 2013].

Deep ocean mooring studies have identified that the seasonal variability of the EGC upstream of the Denmark Strait differs from that found in DSOW [*Jonsson*, 1999; *Jonsson and Valdimarsson*, 2004]. As initially suggested by Swift et al. [1980], recent evidence strongly supports the importance of intermediate waters formed by winter convection in the Iceland Sea as important contributors (~50%) to the DSOW transports [*Vage et al.*, 2011]. For example, the recently discovered North Icelandic Jet (NIJ), is a narrow 15-20 km-wide barotropic jet that flows from the Iceland Sea to the Denmark Strait along the Iceland Slope beneath the Atlantic inflow branch with a mean speed velocity of 40 cm/sec following the 600 m isobath [*Jonsson and Valdimarsson*, 2004]. As demonstrated in model simulations, the transport and transformation of the warm salty waters from the North Iceland Irminger Current, a branch of the Atlantic inflow, Figure 1) into the Iceland Basin, plays a critical role in the formation of the NIJ [*Vage et al.*, 2011]. However, Late Holocene reconstructions, based on foraminiferal and coccolithophore assemblages [*Giraudeau et al.*, 2004; *Ólafsdóttir et al.*, 2010; *Jennings et al.*, 2011] show a decrease in the influence NIIC reaching North Iceland for the last 4000 years. This is further supported by alkenone and diatom-based temperature reconstructions from North Iceland [*Jiang et al.*, 2002; *Bendle and Rosell-Mele*, 2007; *Sicre et al.*, 2008b] (Figure 4d). Taken together, these studies consistently suggest a gradual increase in the influence of polar waters relative to Atlantic waters reaching the North Icelandic shelf over the last 3000 years. It is therefore difficult to reconcile an increased

415 influence of fresher polar waters in the Iceland Sea promoting enhanced winter convection,
416 especially since modelling studies have demonstrated the key role of the inflow of Atlantic
417 waters in the preconditioning for open convection in the Iceland Sea [*Vage et al.*, 2011].
418 We therefore argue that an enhanced supply and/or density of the EGC waters to the DSOW
419 is the most plausible explanation for the upstream changes that might have led to a
420 Neoglacial increase in the DSOW vigour as recorded in RAPiD-35-COM. It is possible that
421 the Arctic increase in sea ice formation and sea ice cover during the Neoglacial (as a response
422 to the decrease in summer insolation at high latitudes) could have led to an increase in the
423 formation of dense Arctic waters via brine rejection processes [*Rasmussen and Thomsen*,
424 2014]. Furthermore, it has been proposed that the Mid to Late Holocene was a transition
425 towards a weakened state of the North Atlantic Oscillation (NAO) like atmospheric pattern in
426 the Nordic Seas [*Rimbu et al.*, 2003]. This atmospheric configuration may have promoted the
427 southward transport of EGC waters (Dickson 2000). However, changes in the regional
428 atmospheric circulation over the Neoglaciation remain largely unresolved due to the lack of
429 consistent atmospheric proxy data [e.g. *Mayewski et al.*, 1997; *Nesje et al.*, 2001; *Lamy et al.*,
430 2006; *Olsen et al.*, 2012; *Jackson et al.*, 2005]. Alternatively, the increase in the vigour of
431 DSOW over the last 2300 years, may have instead been caused by downstream processes.
432
433 *6.3.3. Downstream entrainment processes of DSOW*
434 The overflow transport is also driven by the cross-sill density gradient and the hydrography
435 of the water masses lying above the overflows once they enter the Atlantic Basin.
436 Consequently, past changes in the density of the downstream water masses such as SPMW
437 and LSW may also have affected the vigour of the DSOW. Hydrographic transects show that,
438 during periods of reduced (enhanced) LSW formation, the density and volume of this water
439 mass in the Irminger Basin is decreased (increased). A comparison of the millennial-scale

variability of the surface conditions in the Eastern Labrador Sea highlight a millennial-scale cooling of the IC perhaps indicating a weakening in the SPG circulation over the last 2250-3000 years BP and more influence of polar versus Atlantic waters in the WGC [*Perner et al.*, 2011]. This trend is similar to the one recorded in the DSOW vigour towards higher speeds. A Late Holocene decrease in LSW formation (and hence density) would have led to an increase in the cross-ridge density gradient, thereby driving a faster transport of DSOW into the Atlantic Basin, which in turn would also promote entrainment and therefore a greater volume of DSOW.

This finding is in agreement with observational data [*Dickson et al.*, 1996] that have suggested the presence of an antiphased 'see-saw' of deep water formation between the convection centres of the Labrador and Greenland Sea. The relationship has been explained to occur through the opposing impacts of atmospheric circulation in each of the convective centres [*Dickson et al.*, 1996]. This seminal work by Dickson et al. (1996) concluded that during a positive North Atlantic Oscillation (NAO) state the strengthening of the westerlies (more zonal atmospheric circulation) over the North Atlantic promoted heat loss and deep convection in the Labrador Sea. Conversely, during a negative NAO state the enhanced northerlies (more meridional atmospheric and surface circulation in the Nordic Seas-Blinheim [2000]) aided the delivery of polar waters via the EGC into the SPG, thereby inhibiting convection in the Labrador Sea but enhancing it in the Greenland Sea. However, during the Neoglaciation, proxy work from the Fram Strait has suggested an expansion of the sea ice into the Greenland Sea [*Müller et al.*, 2012; *Werner et al.*, 2013], which means that freshwater forcing deriving from an increase in Arctic sea ice export might also have been a dominant control on convection in the Greenland Sea.

6.3.4. Summary of DSOW flow variability

As illustrated above, our current knowledge of the causes of transport variability of DSOW in the modern is still very limited, an issue which complicates our interpretation of the near-bottom flow speed of DSOW in the past. From the options outlined above it is hard to discern which one was the dominant mechanism in governing the millennial trend towards an increased vigour of DSOW from about ~2300 years BP. From the evidence presented, we conclude that upstream changes in the transport and constituents of the EGC and/or a reduction in the LSW formation were the most likely candidates for the Late Holocene strengthening of DSOW. We can additionally conclude that from the evidence presented here it is unlikely that increased NIIC reaching the Iceland Sea had control on the centennial to millennial variability of DSOW. The proposed changes in the Neoglacial ocean conditions were chiefly governed by the insolation-driven increase in Arctic sea ice production and potential changes in atmospheric circulation.

6.4. Potential antiphasing of the Nordic Overflows

The relationship between the vigour of ISOW and DSOW is yet to be fully established. Modelling studies have frequently proposed an antiphasing of the volume transport between these overflows over the GSR, caused by the differing effects of atmospheric forcing on the deep water formation at the different convection sites in the Nordic Seas which supply the overflows [*Biastoch et al.*, 2003; *Kohl*, 2010; *Serra et al.*, 2010; *Sandø et al.*, 2012]. Nonetheless, this relationship has not yet been clearly observed in the instrumental record. The observed weakening of DSOW [*Macrander et al.*, 2005] and strengthening of ISOW [*Hansen and Osterhus*, 2007] in 2000 has been used as evidence for this relationship [*Kohl et al.*, 2007], but there is yet no convincing observational evidence for this co-variance of the overflows.

A visual comparison of the near-bottom flow speed reconstructions from ISOW and DSOW strongly suggests an antiphased relationship between the two records (Figure 5). Indeed, the normalised 45-year Gaussian interpolated $\overline{SS}$ records from ISOW (RAPiD-17-5P) and DSOW (RAPiD-35-COM) shows a Pearson Correlation of -0.417 with a 95% confidence interval of -0.595;-0.182 (note: this correlation coefficient could be increased if these records were tied within their respective age errors to one another) (Figure 5). These findings suggest anti-phased behaviour in the vigour of the overflows east and west of Iceland on a millennial-scale. Although it is not possible to investigate the potential compensation in the cross-ridge volume transport of the overflows caused by this antiphasing, these results are in agreement with numerous modelling results [*Biastoch et al.*, 2003; *Kohl*, 2010; *Serra et al.*, 2010; *Sandø et al.*, 2012]. Initially it was suggested that an increase in wind-stress curl north of Iceland steers the circulation of waters to the west of Iceland enhancing DSOW transport while decreasing the outflow through the Faroe Bank Channel [*Biastoch et al.*, 2003]. However, recent modelling studies propose that this anti-correlated behaviour of the overflows stems from a switch between differently sourced water masses supplying the overflows as a response to wind-stress curl changes around Iceland and in the Nordic Seas (which is closely dependent on the NAO state) [*Kohl*, 2010; *Serra et al.*, 2010]. The mechanism invoking the re-direction of the surface waters east and west of Iceland via wind-stress forcing is probably of more relevance to DSOW variability on annual to shorter time-scales whereas upstream changes in the site of overflow formation are more likely the causes for longer time-scale variability [*Kohl et al.*, 2007].

7. Conclusions

In this paper we have presented the first subdecadal to decadal reconstructions of the vigour of the two Nordic Overflows (ISOW and the DSOW) for the last 3000-4000 years. The results do not show a consistent change in the strength of either of the Nordic Overflows

515 during the well-known centennial climate change events that have been commonly found in
516 the North Atlantic region. Our findings therefore suggest that contrary to previous
517 suggestions, this crucial component of the deep limb of the AMOC was potentially unrelated
518 to the centennial scale climate variability over the Late Holocene [*Bianchi and McCave*,
519 1999]. It is therefore possible that if in fact there is a link between AMOC strength changes
520 and these climatic events, it would have likely involved the formation of deep waters in the
521 Labrador Sea; LSW [*Moffa-Sanchez et al.*, 2014b]. However, a consistent millennial pattern
522 is found in the two reconstructions: a slower ISOW from 1500 years BP to present and a
523 faster DSOW from 2300 years BP. We propose that these millennial trends were caused by
524 the surface alteration of the hydrography and atmospheric re-organisation in the Arctic and
525 Nordic Seas as a response to the decrease in summer Northern Hemisphere insolation through
526 the Neoglaciation. A comparison of the overflow strength east and west of Iceland reveals a
527 striking co-variability. Modelling studies have repeatedly reported an antiphased behaviour of
528 the overflows but evidence for this has so far been limited. As suggested from the model
529 results, it is possible that this antiphased behaviour was driven by atmospheric changes
530 switching the deep water formation sites that contribute to each of the overflows. The anti-
531 phased behaviour of the overflows on multicentennial to millennial timescales could allow
532 for the compensation of the overflows east and west of Iceland, such that there was perhaps
533 little effect on the net transport of deep waters of waters feeding the deep limb of the AMOC
534 over the late Holocene.

535 ## 8. Figure Captions

536 **Figure 1.** Bathymetric map of the Nordic Seas and the North Atlantic indicating the location
537 of RAPiD-17-5P and RAPiD-35-COM (black filled circles indicate the core locations used in
538 this study). Black dashed fine lines indicate the Greenland-Scotland Ridge. Dark blue arrows
539 represent the simplified deep ocean circulation of the Nordic Sea Overflows, ISOW and

DSOW and DWBC. Spirals indicate the sites of open ocean convection in the Nordic Seas, which feed the Nordic Overflows. The surface ocean circulation is represented by the dashed arrows, the pink indicating waters that originate from the North Atlantic Current (NAC), the Norwegian Atlantic Current (NwAC) and the light blue represent the polar-derived currents such as the East Greenland Current (EGC) and the East Icelandic Current (EIC). Base map adapted from Ocean Data View [*Schlitzer*, 2014].

Figure 2. Core-chronology for RAPiD-35-14P based on ten calibrated radiocarbon dates (filled black circles). The age–model was constructed using a bayesian age-model programme; BChron [*Haslett and Parnell*, 2008]. The light grey shaded area indicates the 95% probability error within the age model calculated in BChron. The light blue vertical band indicates the area where the data from the box-core RAPiD-35-25B (Moffa-Sanchez et al. 2014b) was used and spliced.

Figure 3. (a) Insolation at 60^{o}N , (b) δ^{18}O measurements on Neogloboquadrina dextral which are indicative of sea surface temperatures [*Sejrup et al.*, 2011] **(**c) % Quartz recorded from the North Icelandic shelf [*Moros et al.*, 2006], (d) Greenland Ice Sheet Project 2 temperature reconstructions from Greenland [*Alley et al.*, 2000], (e) $\overline{SS}$ measurements from RAPiD-17-5P (this study). Inset map shows the colour-coded core locations of the records presented in the graph. Red and blue horizontal bars indicate the warm and cold periods respectively in the circum-North Atlantic [*Mayewski*, 2004]. Grey vertical shaded areas mark the time periods were $\overline{SS}$ values were below the average record values.

Figure 4. (a) Near-bottom flow speed vigour of DSOW ($\overline{SS}$ measurements from RAPiD-35-COM-this study) (b) Number of IRD grains >2mm from the East Greenland Coast [*Jennings*

565 *et al.*, 2002], (c) % quartz from the North Icelandic shelf [*Moros et al.*, 2006], (d) alkenone-
566 based August Sea Surface Temperatures (SST) from North Iceland [*Sicre et al.*, 2008a,
567 2008b]. Arrows highlight the millennial-scale trends. Inset map shows the colour coded core
568 locations of the proxy reconstructions presented in the figure. Red and blue horizontal bars
569 mark the warm and cold periods respectively in the circum-North Atlantic [*Mayewski*, 2004].
570 Grey vertical shaded areas mark the time periods were $\overline{SS}$ values were below average.
571
572 **Figure 5.** Comparison between the $\overline{SS}$ records from DSOW (RAPiD-35-COM) and ISOW
573 (RAPiD-17-5P) in black and red respectively, which reveals antiphasing of the near-bottom
574 flow speeds for the last 3000 years. Lower panels normalised 45-gaussian smoothed $\overline{SS}$ data
575 from ISOW and DSOW changes with time (left), versus each other (right).
576

577 9. Acknowledgements

578 We thank the crew of *RV Charles Darwin 159*. We also thank the insightful and careful
579 comments of two anonymous reviewers. The radiocarbon dating was supported by funding
580 from the National Environment Research Countil U.K. P.M. and I.H. gratefully acknowledge
581 the support of the Climate Change Consortium of Wales (www.c3wales.org).
582

583 10. References

584 Van Aken, H. M., and G. Becker (1996), Hydrography and through-flow in the north-eastern
585 North Atlantic Ocean: the NANSEN project, *Prog. Oceanogr.*, *38*(4), 297–346,
586 doi:10.1016/s0079-6611(97)00005-0.

587 Van Aken, H. M. (1995), HYDROGRAPHIC VARIABILITY IN THE BOTTOM LAYER
588 OF THE ICELAND BASIN, *J. Phys. Oceanogr.*, *25*(7), 1716–1722,
589 doi:10.1175/1520-0485(1995)025<1716:hvitbl>2.0.co;2.

590 Alley, R. B. (2000), The Younger Dryas cold interval as viewed from central Greenland,
591 *Quat. Sci. Rev.*, *19*(1-5), 213–226, doi:10.1016/S0277-3791(99)00062-1.

592 Andersen, C., N. Koç, A. Jennings, and J. T. Andrews (2004), Nonuniform response of the
593 major surface currents in the Nordic Seas to insolation forcing: Implications for the
594 Holocene climate variability, *Paleoceanography*, *19*(2), PA2003,
595 doi:10.1029/2002pa000873.

596 Andersson, C., F. S. R. Pausata, E. Jansen, B. Risebrobakken, and R. J. Telford (2010),
597 Holocene trends in the foraminifer record from the Norwegian Sea and the North
598 Atlantic Ocean, *Clim. Past*, *6*(2), 179–193.

599 Andrews, J. T. (2009), Seeking a Holocene drift ice proxy: Non-clay mineral variations from
600 the SW to N-central Iceland shelf: Trends, regime shifts, and periodicities, *J. Quat.*
601 *Sci.*, *24*(7), 664–676, doi:10.1002/jqs.1257.

602 Andrews, J. T., L. M. Smith, R. Preston, T. Cooper, and A. E. Jennings (1997), Spatial and
603 temporal patterns of iceberg rafting (IRD) along the East Greenland margin, ca. 68°N,
604 over the last 14 cal.ka, *J. Quat. Sci.*, *12*(1), 1–13.

605 Bendle, J. A. P., and A. Rosell-Mele (2007), High-resolution alkenone sea surface
606 temperature variability on the North Icelandic Shelf: implications for Nordic Seas
607 palaeoclimatic development during the Holocene, *Holocene*, *17*(1), 9–24,
608 doi:10.1177/0959683607073269.

609 Bianchi, G. G., and I. N. McCave (1999), Holocene periodicity in North Atlantic climate and
610 deep-ocean flow south of Iceland, *Nature*, *397*(6719), 515–517, doi:10.1038/17362.

611 Bianchi, G. G., and I. N. McCave (2000), Hydrography and sedimentation under the deep
612 western boundary current on Björn and Gardar Drifts, Iceland Basin, *Mar. Geol.*,
613 *165*(1–4), 137–169, doi:10.1016/s0025-3227(99)00139-5.

614 Bianchi, G. G., I. R. Hall, I. N. McCave, and L. Joseph (1999), Measurement of the sortable
615 silt current speed proxy using the Sedigraph 5100 and Coulter Multisizer IIe:
616 Precision and accuracy, *Sedimentology*, *46*(6), 1001–1014.

617 Biastoch, A., R. H. Kase, and D. B. Stammer (2003), The sensitivity of the Greenland-
618 Scotland Ridge overflow to forcing changes, *J. Phys. Oceanogr.*, *33*(11), 2307–2319,
619 doi:10.1175/1520-0485(2003)033<2307:tsotgr>2.0.co;2.

620 Blindheim, J., V. Borovkov, B. Hansen, S. A. Malmberg, W. R. Turrell, and S. Osterhus
621 (2000), Upper layer cooling and freshening in the Norwegian Sea in relation to
622 atmospheric forcing, *Deep-Sea Res. Part -Oceanogr. Res. Pap.*, *47*(4), 655–680,
623 doi:10.1016/s0967-0637(99)00070-9.

624 Boessenkool, K. P., I. R. Hall, H. Elderfield, and I. Yashayaev (2007), North Atlantic climate
625 and deep-ocean flow speed changes during the last 230 years, *Geophys. Res. Lett.*,
626 *34*(13), L13614, doi:10.1029/2007gl030285.

627 Born, A., A. Levermann, and J. Mignot (2009), Sensitivity of the Atlantic Ocean circulation
628 to a hydraulic overflow parameterisation in a coarse resolution model: Response of
629 the subpolar gyre, *Ocean Model.*, *27*(3–4), 130–142,
630 doi:10.1016/j.ocemod.2008.11.006.

631 Calvo, E., J. O. Grimalt, and E. Jansen (2002), High resolution U(37)(K) sea surface
632 temperature reconstruction in the Norwegian Sea during the Holocene, *Quat. Sci.*
633 *Rev.*, *21*(12-13), 1385–1394, doi:10.1016/s0277-3791(01)00096-8.

634 Delworth, T. L., and M. E. Mann (2000), Observed and simulated multidecadal variability in
635 the Northern Hemisphere, *Clim. Dyn.*, *16*(9), 661–676, doi:10.1007/s003820000075.

636 Denton, G. H., and W. Karlén (1973), Holocene climatic variations—Their pattern and
637 possible cause, *Quat. Res.*, *3*(2), 155–205, doi:10.1016/0033-5894(73)90040-9.

638 Dickson, B., J. Meincke, and P. Rhines (2008), *Arctic–Subarctic Ocean Fluxes Defining the*
639 *Role of the Northern Seas in Climate*, The Inflow of Atlantic Water, Heat, and Salt to
640 the Nordic Seas Across the Greenland–Scotland Ridge, Springer Netherlands.

641 Dickson, R., J. Lazier, J. Meincke, P. Rhines, and J. Swift (1996), Long-term coordinated
642 changes in the convective activity of the North Atlantic, *Prog. Oceanogr.*, *38*(3), 241–
643 295.

644 Dickson, R. R., and J. Brown (1994), The production of North Atlantic Deep Water: Sources,
645 rates, and pathways, *J Geophys Res*, *99*(C6), 12319–12341, doi:10.1029/94jc00530.

646 Eldevik, T., J. E. O. Nilsen, D. Iovino, K. Anders Olsson, A. B. Sando, and H. Drange
647 (2009), Observed sources and variability of Nordic seas overflow, *Nat. Geosci.*, *2*(6),
648 406–410, doi:10.1038/ngeo518.

649 Ellison, C. R. W., M. R. Chapman, and I. R. Hall (2006), Surface and Deep Ocean
650 Interactions During the Cold Climate Event 8200 Years Ago, *Science*, *312*(5782),
651 1929–1932, doi:10.1126/science.1127213.

652 Fagel, N., C. Hillaire-Marcel, M. Humblet, R. Brasseur, D. Weis, and R. Stevenson (2004),
653 Nd and Pb isotope signatures of the clay-size fraction of Labrador Sea sediments
654 during the Holocene: Implications for the inception of the modern deep circulation
655 pattern, *Paleoceanography*, *19*(3), PA3002, doi:10.1029/2003PA000993.

656 Fogelqvist, E., J. Blindheim, T. Tanhua, S. Osterhus, E. Buch, and F. Rey (2003), Greenland-
657 Scotland overflow studied by hydro-chemical multivariate analysis, *Deep-Sea Res.*
658 *Part -Oceanogr. Res. Pap.*, *50*(1), 73–102, doi:10.1016/s0967-0637(02)00131-0.

659 Giraudeau, J., A. E. Jennings, and J. T. Andrews (2004), Timing and mechanisms of surface
660 and intermediate water circulation changes in the Nordic Seas over the last 10,000
661 years: a view from the North Iceland shelf, *Quat. Sci. Rev.*, *23*(20–22), 2127–2139,
662 doi:10.1016/j.quascirev.2004.08.011.

663 Gray, S. T., L. J. Graumlich, J. L. Betancourt, and G. T. Pederson (2004), A tree-ring based
664 reconstruction of the Atlantic Multidecadal Oscillation since 1567 AD, *Geophys. Res.*
665 *Lett.*, *31*(12), doi:10.1029/2004gl019932.

666 Hall, I. R., G. G. Bianchi, and J. R. Evans (2004), Centennial to millennial scale Holocene
667 climate-deep water linkage in the North Atlantic, *Quat. Sci. Rev.*, *23*(14-15), 1529–
668 1536.

669 Hansen, B., and S. Osterhus (2007), Faroe Bank Channel overflow 1995-2005, *Prog.*
670 *Oceanogr.*, *75*(4), 817–856, doi:10.1016/j.pocean.2007.09.004.

671 Hansen, B., W. R. Turrell, and S. Osterhus (2001), Decreasing overflow from the Nordic seas
672 into the Atlantic Ocean through the Faroe Bank channel since 1950, *Nature*,
673 *411*(6840), 927–930, doi:10.1038/35082034.

674 Hansen, B., S. Østerhus, D. Quadfasel, and W. Turrell (2004), Already the Day After
675 Tomorrow?, *Science*, *305*(5686), 953–954, doi:10.1126/science.1100085.

676 Hansen, B., H. Hátún, R. Kristiansen, S. M. Olsen, and S. Østerhus (2010), Stability and
677 forcing of the Iceland-Faroe inflow of water, heat, and salt to the Arctic, ., 6, 1013-
678 1026, doi:10.5194/os-6-1013-2010, 2010., , *6*, 1013–1026.

679 Haslett, J., and A. Parnell (2008), A simple monotone process with application to
680 radiocarbon-dated depth chronologies, *J. R. Stat. Soc. Ser. C Appl. Stat.*, *57*(4), 399–
681 418, doi:10.1111/j.1467-9876.2008.00623.x.

682 Holliday, N. P., S. Bacon, J. Allen, and E. L. McDonagh (2009), Circulation and transport in
683 the western boundary currents at Cape Farewell, Greenland, *J. Phys. Oceanogr.*,
684 *39*(8), 1854–1870, doi:10.1175/2009JPO4160.1.

685 Jackson, M. G., N. Oskarsson, R. G. Trønnes, J. F. McManus, D. W. Oppo, K. Grönvold, S.
686 R. Hart, and J. P. Sachs (2005), Holocene loess deposition in Iceland: Evidence for
687 millennial-scale atmosphere-ocean coupling in the North Atlantic, *Geology*, *33*(6),
688 509–512.

689 Jeansson, E., S. Jutterstroem, B. Rudels, L. G. Anderson, K. A. Olsson, E. P. Jones, W. M.
690 Smethie, and J. H. Swift (2008), Sources to the East Greenland Current and its
691 contribution to the Denmark Strait Overflow, *Prog. Oceanogr.*, *78*(1), 12–28,
692 doi:10.1016/j.pocean.2007.08.031.

693 Jennings, A., J. Andrews, and L. Wilson (2011), Holocene environmental evolution of the SE
694 Greenland Shelf North and South of the Denmark Strait: Irminger and East Greenland
695 current interactions, *Quat. Sci. Rev.*, *30*(7-8), 980–998.

696 Jennings, A. E., K. L. Knudsen, M. Hald, C. V. Hansen, and J. T. Andrews (2002), A mid-
697 Holocene shift in Arctic sea-ice variability on the East Greenland Shelf, *Holocene*,
698 *12*(1), 49–58.

699 Jiang, H., M. S. Seidenkrantz, K. L. Knudsen, and J. Eiriksson (2002), Late-Holocene
700 summer sea-surface temperatures based on a diatom record from the north Icelandic
701 shelf, *Holocene*, *12*(2), 137–147, doi:10.1191/0959683602h1529rp.

702 Jonsson, S. (1999), The circulation in the northern part of the Denmark Strait and its
703 variability, *CES CM*, *9*.

704 Jonsson, S., and H. Valdimarsson (2004), A new path for the Denmark Strait overflow water
705 from the Iceland Sea to Denmark Strait, *Geophys. Res. Lett.*, *31*(3), L03305,
706 doi:10.1029/2003gl019214.

707 Kissel, C., A. Van Toer, C. Laj, E. Cortijo, and E. Michel (2013), Variations in the strength
708 of the North Atlantic bottom water during Holocene, *Earth Planet. Sci. Lett.*, *369–*
709 *370*(0), 248–259, doi:10.1016/j.epsl.2013.03.042.

710 Knight, J. R., R. J. Allan, C. K. Folland, M. Vellinga, and M. E. Mann (2005), A signature of
711 persistent natural thermohaline circulation cycles in observed climate, *Geophys. Res.*
712 *Lett.*, *32*(20), doi:10.1029/2005gl024233.

713 Kobashi, T., K. Kawamura, J. P. Severinghaus, J. Barnola, T. Nakaegawa, B. M. Vinther, S.
714 J. Johnsen, and J. E. Box (2011), High variability of Greenland surface temperature
715 over the past 4000 years estimated from trapped air in an ice core, *Geophys. Res.*
716 *Lett.*, *38*(21).

717 Kohl, A. (2010), Variable source regions of Denmark Strait and Faroe Bank Channel
718 overflow waters, *Tellus Ser. -Dyn. Meteorol. Oceanogr.*, *62*(4), 551–568,
719 doi:10.1111/j.1600-0870.2010.00454.x.

720 Kohl, A., R. H. Kaese, D. Stammer, and N. Serra (2007), Causes of changes in the Denmark
721 strait overflow, *J. Phys. Oceanogr.*, *37*(6), 1678–1696, doi:10.1175/jpo3080.1.

722 Kuhlbrodt, T., A. Griesel, M. Montoya, A. Levermann, M. Hofmann, and S. Rahmstorf
723 (2007), On the driving processes of the Atlantic meridional overturning circulation,
724 *Rev. Geophys.*, *45*(2), RG2001, doi:10.1029/2004RG000166.

725 Lamy, F., H. W. Arz, G. C. Bond, A. Bahr, and J. Pätzold (2006), Multicentennial-scale
726 hydrological changes in the Black Sea and northern Red Sea during the Holocene and
727 the Arctic/North Atlantic Oscillation, *Paleoceanography*, *21*(1), PA1008,
728 doi:10.1029/2005PA001184.

729 Lohmann, K., J. Mignot, H. R. Langehaug, J. H. Jungclaus, D. Matei, O. H. Otterå, Y. Gao,
730 T. L. Mjell, U. Ninnemann, and H. F. Kleiven (2014), Using simulations of the last
731 millennium to understand climate variability seen in paleo-observations: similar
732 variation of Iceland-Scotland overflow strength and Atlantic Multidecadal Oscillation,
733 *Clim Past Discuss*, *10*(4), 3255–3302, doi:10.5194/cpd-10-3255-2014.

734 Macrander, A., U. Send, H. Valdimarsson, S. Jónsson, and R. H. Käse (2005), Interannual
735 changes in the overflow from the Nordic Seas into the Atlantic Ocean through
736 Denmark Strait, *Geophys. Res. Lett.*, *32*(6), L06606, doi:10.1029/2004gl021463.

737 Mann, M. E., and J. M. Lees (1996), Robust estimation of background noise and signal
738 detection in climatic time series, *Clim. Change*, *33*(3), 409–445,
739 doi:10.1007/bf00142586.

740 Mann, M. E., Z. Zhang, S. Rutherford, R. S. Bradley, M. K. Hughes, D. Shindell, C.
741 Ammann, G. Faluvegi, and F. Ni (2009), Global Signatures and Dynamical Origins of
742 the Little Ice Age and Medieval Climate Anomaly, *Science*, *326*(5957), 1256–1260,
743 doi:10.1126/science.1177303.

744 Mauritzen, C. (1996), Production of dense overflow waters feeding the North Atlantic across
745 the Greenland-Scotland Ridge. Part 1: Evidence for a revised circulation scheme,
746 *Deep Sea Res. Part Oceanogr. Res. Pap.*, *43*(6), 769–806, doi:10.1016/0967-
747 0637(96)00037-4.

748 Mayewski, P. A. (2004), Holocene climate variability, *Quat Res*, *62*, 243–255,
749 doi:10.1016/j.yqres.2004.07.001.

750 Mayewski, P. A., L. D. Meeker, M. S. Twickler, S. Whitlow, Y. Qinzhao, W. Berry Lyons,
751 and M. Prentice (1997), Major features and forcing of high-latitude Northern
752 Hemisphere atmospheric circulation using a 110 000-year-long glaciochemical series,
753 *J. Geophys. Res.*, *102*(C12), 26345–26366.

754 McCave, I. N. (2004), *CD159 Cruise Report*.

755 McCave, I. N., and I. R. Hall (2006), Size sorting in marine muds: Processes, pitfalls, and
756 prospects for paleoflow-speed proxies, *Geochem. Geophys. Geosystems*, *7*(10),
757 Q10N05, doi:10.1029/2006gc001284.

758 McCave, I. N., B. Manighetti, and S. G. Robinson (1995), Sortable Silt and Fine Sediment
759 Size/Composition Slicing: Parameters for Palaeocurrent Speed and
760 Palaeoceanography, *Paleoceanography*, *10*(3), 593–610, doi:10.1029/94pa03039.

761 Meincke, J. (1983), The Modern Current Regime Across the Greenland-Scotland Ridge, in
762 *Structure and Development of the Greenland-Scotland Ridge*, vol. 8, edited by M. P.
763 Bott, S. Saxov, M. Talwani, and J. Thiede, pp. 637–650, Springer US.

764 Moffa-Sanchez, P., A. Born, I. R. Hall, and D. J. R. Thornalley (2014a), Solar forcing of
765 North Atlantic surface temperature and salinity over the last millennium, *Nat. Geosci.*

766 Moffa-Sanchez, P., I. R. Hall, S. Barker, D. J. R. Thornalley, and I. Yashayaev (2014b),
767 Surface changes in the Eastern Labrador Sea around the onset of the Little Ice Age,
768 *Paleoceanography*, doi:10.1002/2013PA002523.

769 Moros, M., K. Emeis, B. Risebrobakken, I. Snowball, A. Kuijpers, J. McManus, and E.
770 Jansen (2004), Sea surface temperatures and ice rafting in the Holocene North
771 Atlantic: climate influences on northern Europe and Greenland, *Quat. Sci. Rev.*,
772 *23*(20–22), 2113–2126, doi:10.1016/j.quascirev.2004.08.003.

773 Moros, M., J. T. Andrews, D. D. Eberl, and E. Jansen (2006), Holocene history of drift ice in
774 the northern North Atlantic: Evidence for different spatial and temporal modes,
775 *Paleoceanography*, *21*(2), doi:10.1029/2005PA001214.

776 Mudelsee, M. (2003), Estimating Pearson's correlation coefficient with bootstrap confidence
777 interval from serially dependent time series, *Math. Geol.*, *35*(6), 651–665.

778 Müller, J., K. Werner, R. Stein, K. Fahl, M. Moros, and E. Jansen (2012), Holocene cooling
779 culminates in sea ice oscillations in Fram Strait, *Quat. Sci. Rev.*, *47*(0), 1–14,
780 doi:10.1016/j.quascirev.2012.04.024.

781 Nesje, A., J. A. Matthews, S. O. Dahl, M. S. Berrisford, and C. Andersson (2001), Holocene
782 glacier fluctuations of Flatebreen and winter-precipitation changes in the
783 Jostedalsbreen region, western Norvay, based on glaciolacustrine sediment records,
784 *The Holocene*, *11*(3), 267–280.

785 Ólafsdóttir, S., A. E. Jennings, A. Geirsdóttir, J. Andrews, and G. H. Miller (2010), Holocene
786 variability of the North Atlantic Irminger current on the south- and northwest shelf of
787 Iceland, *Mar. Micropaleontol.*, *77*(3-4), 101–118.

788 Olsen, J., N. J. Anderson, and M. F. Knudsen (2012), Variability of the North Atlantic
789 Oscillation over the past 5,200 years, *Nat. Geosci*, *5*(11), 808–812.

790 Olsen, S. M., B. Hansen, D. Quadfasel, and S. Osterhus (2008), Observed and modelled
791 stability of overflow across the Greenland-Scotland ridge, *Nature*, *455*(7212), 519–
792 522.

793 Pardoiguzquiza, E., M. Chicaolmo, and F. J. Rodrigueztovar (1994), CYSTRATI - A
794 COMPUTER-PROGRAM FOR SPECTRAL-ANALYSIS OF STRATIGRAPHIC
795 SUCCESSIONS, *Comput. Geosci.*, *20*(4), 511–584, doi:10.1016/0098-
796 3004(94)90080-9.

797 Parnell, A. C., C. E. Buck, and T. K. Doan (2011), A review of statistical chronology models
798 for high-resolution, proxy-based Holocene palaeoenvironmental reconstruction, *Quat.*
799 *Sci. Rev.*, *30*(21–22), 2948–2960, doi:10.1016/j.quascirev.2011.07.024.

800 Perner, K., M. Moros, J. M. Lloyd, A. Kuijpers, R. J. Telford, and J. Harff (2011), Centennial
801 scale benthic foraminiferal record of late Holocene oceanographic variability in Disko
802 Bugt, West Greenland, *Quat. Sci. Rev.*, *30*(19-20), 2815–2826.

803 Price, J. F., and M. O. Baringer (1994), OUTFLOWS AND DEEP-WATER PRODUCTION
804 BY MARGINAL SEAS, *Prog. Oceanogr.*, *33*(3), 161–200, doi:10.1016/0079-
805 6611(94)90027-2.

806 Rahmstorf, S., J. E. Box, G. Feulner, M. E. Mann, A. Robinson, S. Rutherford, and E. J.
807 Schaffernicht (2015), Exceptional twentieth-century slowdown in Atlantic Ocean
808 overturning circulation, *Nat. Clim Change*, *5*(5), 475–480.

809 Rasmussen, T. L., and E. Thomsen (2014), Brine formation in relation to climate changes and
810 ice retreat during the last 15,000 years in Storfjorden, Svalbard, 76–78°N,
811 *Paleoceanography*, *29*(10), 2014PA002643, doi:10.1002/2014PA002643.

812 Reimer, P. J. et al. (2013), IntCal13 and Marine13 Radiocarbon Age Calibration Curves 0–
813 50,000 Years cal BP, *Radiocarb. Vol 55 No 4 2013*.

814 Renssen, H., H. Goosse, and T. Fichefet (2005), Contrasting trends in North Atlantic deep-
815 water formation in the Labrador Sea and Nordic Seas during the Holocene, *Geophys.*
816 *Res. Lett.*, *32*(8), L08711, doi:10.1029/2005GL022462.

817 Rimbu, N., G. Lohmann, J. H. Kim, H. W. Arz, and R. Schneider (2003), Arctic/North
818 Atlantic Oscillation signature in Holocene sea surface temperature trends as obtained
819 from alkenone data, *Geophys. Res. Lett.*, *30*(6), 1280, doi:10.1029/2002gl016570.

820 Risebrobakken, B., E. Jansen, C. Andersson, E. Mjelde, and K. Hevrøy (2003), A high-
821 resolution study of Holocene paleoclimatic and paleoceanographic changes in the
822 Nordic Seas, *Paleoceanography*, *18*(1), 17–1.

Risebrobakken, B., M. Moros, E. V. Ivanova, N. Chistyakova, and R. Rosenberg (2010), Climate and oceanographic variability in the SW Barents Sea during the Holocene, *Holocene*, *20*(4), 609–621, doi:10.1177/0959683609356586.

Rossby, T. (1996), The North Atlantic Current and surrounding waters: At the crossroads, *Rev. Geophys.*, *34*(4), 463–481, doi:10.1029/96RG02214.

Rudels, B., E. Fahrbach, J. Meincke, G. Budeus, and P. Eriksson (2002), The East Greenland Current and its contribution to the Denmark Strait overflow, *Ices J. Mar. Sci.*, *59*(6), 1133–1154, doi:10.1006/jmsc.2002.1284.

Sandø, A. B., J. E. Ø. Nilsen, T. Eldevik, and M. Bentsen (2012), Mechanisms for variable North Atlantic–Nordic seas exchanges, *J. Geophys. Res. Oceans*, *117*(C12), C12006, doi:10.1029/2012JC008177.

Schlesinger, M. E., and N. Ramankutty (1994), An oscillation in the global climate system of period 65-70 years, *Nature*, *367*(6465), 723–726, doi:10.1038/367723a0.

Schlitzer, R. (2014), *Ocean Data View*, Ocean Data View, http://odv.awi.de.

Sejrup, H. P., H. Haflidason, and J. T. Andrews (2011), A Holocene North Atlantic SST record and regional climate variability, *Quat. Sci. Rev.*, *30*(21-22), 3181–3195, doi:10.1016/j.quascirev.2011.07.025.

Serra, N., R. H. KÄSe, A. KÖHl, D. Stammer, and D. Quadfasel (2010), On the low-frequency phase relation between the Denmark Strait and the Faroe-Bank Channel overflows, *Tellus A*, *62*(4), 530–550, doi:10.1111/j.1600-0870.2010.00445.x.

Sicre, M. A., J. Jacob, U. Ezat, S. Rousse, C. Kissel, P. Yiou, J. Eiríksson, K. L. Knudsen, E. Jansen, and J. L. Turon (2008a), Decadal variability of sea surface temperatures off North Iceland over the last 2000 years, *Earth Planet. Sci. Lett.*, *268*(1-2), 137–142, doi:10.1016/j.epsl.2008.01.011.

Sicre, M.-A., P. Yiou, J. Eiriksson, U. Ezat, E. Guimbaut, I. Dahhaoui, K.-L. Knudsen, E. Jansen, and J.-L. Turon (2008b), A 4500-year reconstruction of sea surface temperature variability at decadal time-scales off North Iceland, *Quat. Sci. Rev.*, *27*(21-22), 2041–2047, doi:10.1016/j.quascirev.2008.08.009.

Stocker, T. F., D. Qin, G.-K. Plattner, M. Tignor, S. K. Allen, A. Boschung, A. Nauels, Y. Xia, V. Bex, and P. M. Midgley (2013), *IPCC, 2013: Climate Change 2013: The Physical Science Basis. Contribution of Working Group I to the Fifth Assessment Report of the Intergovernmental Panel on Climate Change*, Cambridge University Press, Cambridge., Cambridge, United Kingdom and New York, NY, USA.

Strass, V. H., E. Fahrbach, U. Schauer, and L. Sellmann (1993), FORMATION OF DENMARK STRAIT OVERFLOW WATER BY MIXING IN THE EAST GREENLAND CURRENT, *J. Geophys. Res.-Oceans*, *98*(C4), 6907–6919, doi:10.1029/92jc02732.

Swift, J. H., and K. Aagaard (1981), Seasonal transitions and water mass formation in the Iceland and Greenland seas, *Deep Sea Res. Part Oceanogr. Res. Pap.*, *28*(10), 1107–1129, doi:10.1016/0198-0149(81)90050-9.

Swift, J. H., K. Aagaard, and S. A. Malmberg (1980), CONTRIBUTION OF THE DENMARK STRAIT OVERFLOW TO THE DEEP NORTH-ATLANTIC, *Deep-Sea Res. Part -Oceanogr. Res. Pap.*, *27*(1), 29–42, doi:10.1016/0198-0149(80)90070-9.

Tanhua, T., K. A. Olsson, and E. Jeansson (2005), Formation of Denmark Strait overflow water and its hydro-chemical composition, *J. Mar. Syst.*, *57*(3-4), 264–288, doi:10.1016/j.jmarsys.2005.05.003.

Thornalley, D. J. R., H. Elderfield, and I. N. McCave (2010), Intermediate and deep water paleoceanography of the northern North Atlantic over the past 21,000 years, *Paleoceanography*, *25*(1), PA1211, doi:10.1029/2009PA001833.

Thornalley, D. J. R., M. Blaschek, F. J. Davies, S. Praetorius, D. W. Oppo, J. F. McManus, I. R. Hall, H. Kleiven, H. Renssen, and I. N. McCave (2013), Long-term variations in Iceland–Scotland overflow strength during the Holocene, *Clim Past*, *9*(5), 2073–2084, doi:10.5194/cp-9-2073-2013.

Torrence, C., and G. P. Compo (1998), A Practical Guide to Wavelet Analysis, *Bull. Am. Metereological Soc.*, *79*, 61–78.

Vage, K., R. S. Pickart, M. A. Spall, H. Valdimarsson, S. Jonsson, D. J. Torres, S. Osterhus, and T. Eldevik (2011), Significant role of the North Icelandic Jet in the formation of Denmark Strait overflow water, *Nat. Geosci*, *4*(10), 723–727.

Våge, K., R. S. Pickart, M. A. Spall, G. W. K. Moore, H. Valdimarsson, D. J. Torres, S. Y. Erofeeva, and J. E. Ø. Nilsen (2013), Revised circulation scheme north of the Denmark Strait, *Deep Sea Res. Part Oceanogr. Res. Pap.*, *79*(0), 20–39, doi:10.1016/j.dsr.2013.05.007.

Vellinga, M., and P. Wu (2004), Low-Latitude Freshwater Influence on Centennial Variability of the Atlantic Thermohaline Circulation, *J. Clim.*, *17*(23), 4498–4511, doi:10.1175/3219.1.

Werner, K., R. F. Spielhagen, D. Bauch, H. C. Hass, and E. Kandiano (2013), Atlantic Water advection versus sea-ice advances in the eastern Fram Strait during the last 9 ka: Multiproxy evidence for a two-phase Holocene, *Paleoceanography*, *28*(2), 283–295, doi:10.1002/palo.20028.

Whitehead, J. A. (1998), Topographic control of oceanic flows in deep passages and straits, *Rev. Geophys.*, *36*(3), 423–440, doi:10.1029/98rg01014.

Wilkenskjeld, S., and D. Quadfasel (2005), Response of the Greenland-Scotland overflow to changing deep water supply from the Arctic Mediterranean, *Geophys. Res. Lett.*, *32*(21), L21607, doi:10.1029/2005gl024140.

Zhang, R., T. L. Delworth, A. Rosati, W. G. Anderson, K. W. Dixon, H.-C. Lee, and F. Zeng (2011), Sensitivity of the North Atlantic Ocean Circulation to an abrupt change in the Nordic Sea overflow in a high resolution global coupled climate model, *J. Geophys. Res.*, *116*(C12), C12024, doi:10.1029/2011jc007240.

Figure 1

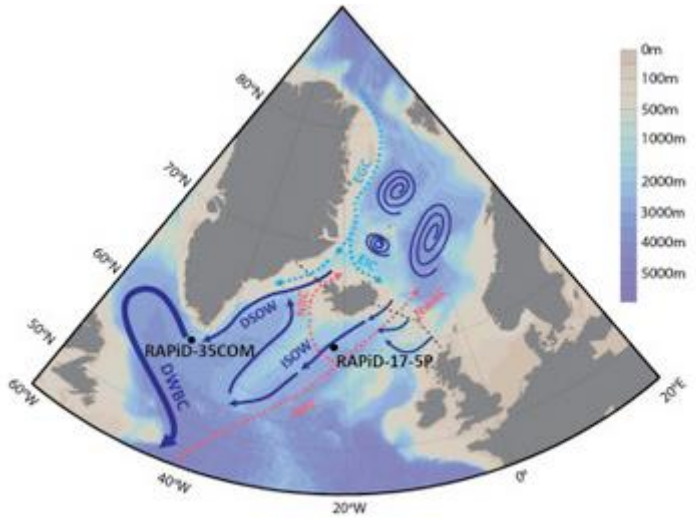

Figure 2

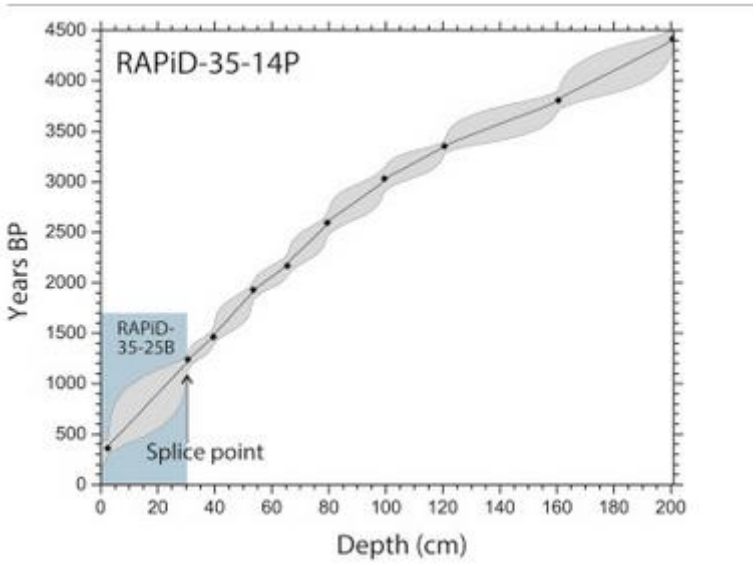

Figure 3

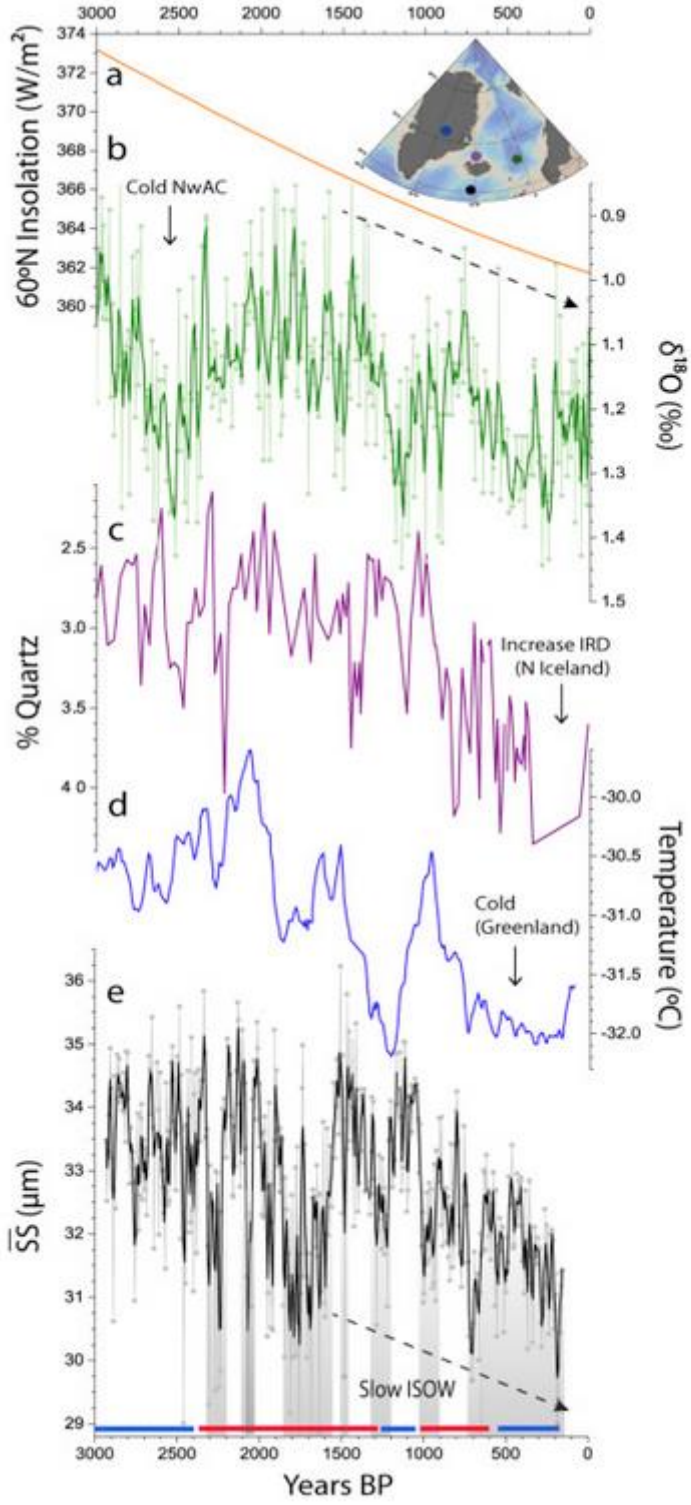
3000
2500
2000
1500
1000
500
0
a
b
c
d
e
60°N Insolation (W/m²)
Cold NwAC
δ18O (‰)
% Quartz
Increase IRD
(N Iceland)
Temperature (°C)
Cold
(Greenland)
SS̄ (μm)
Slow ISOW
Years BP

Figure 4

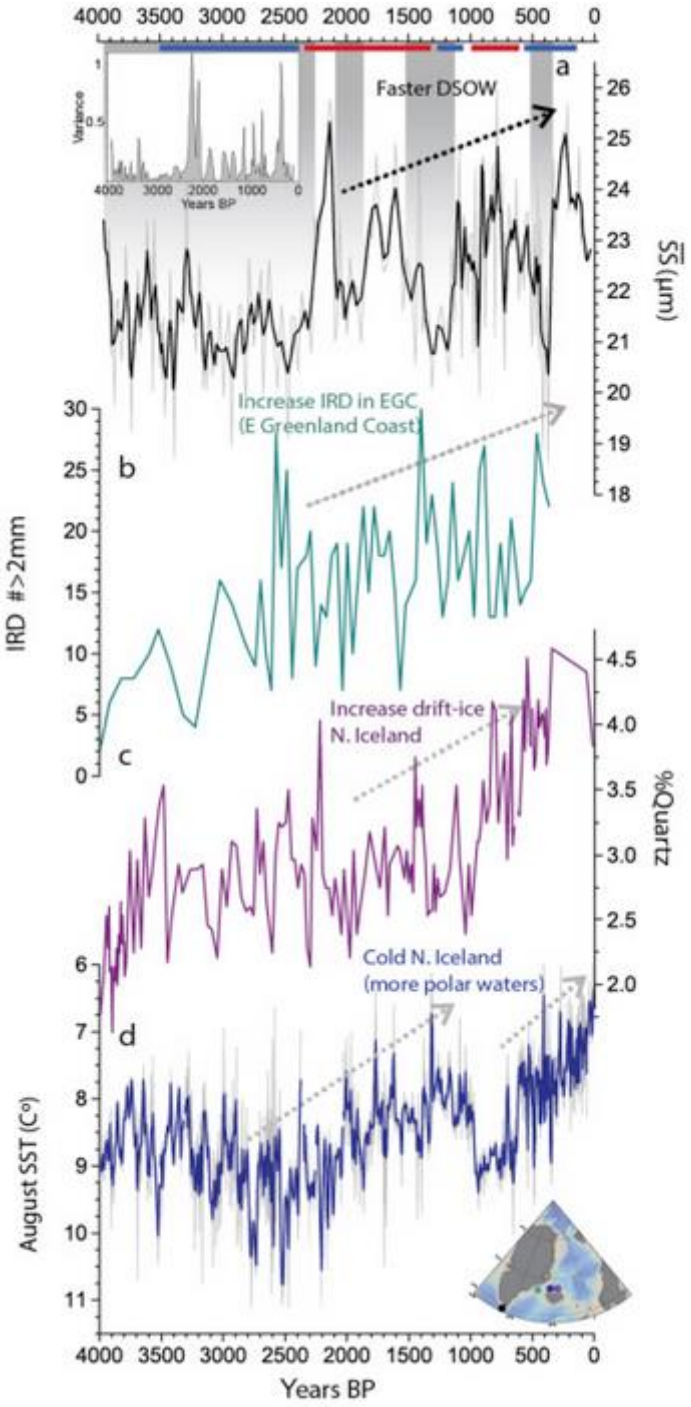
4000 3500 3000 2500 2000 1500 1000 500 0
a
Faster DSOW
Variance
Years BP
SS̄ (µm)
Increase IRD in EGC
(E Greenland Coast)
b
IRD #>2mm
Increase drift-ice
N. Iceland
c
%Quartz
Cold N. Iceland
(more polar waters)
d
August SST (C°)
Years BP

Figure 5

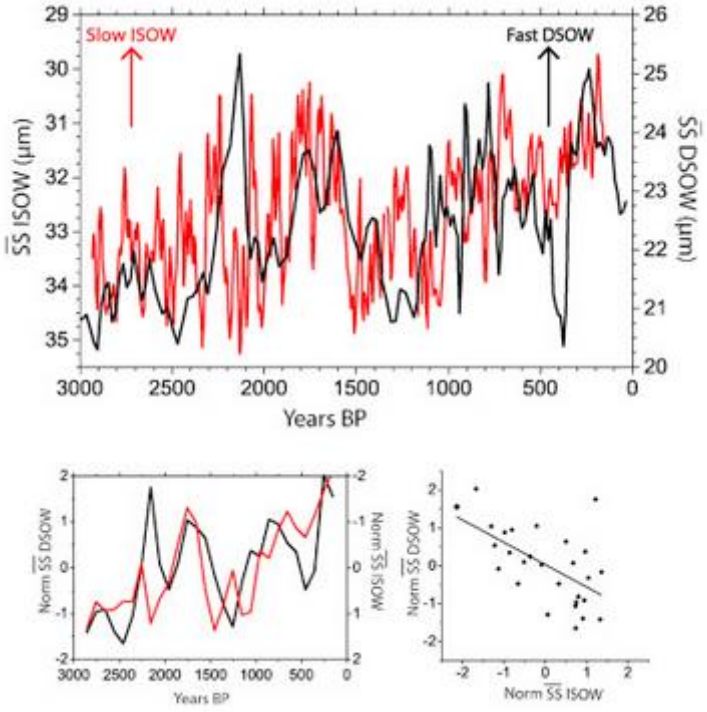
Slow ISOW
Fast DSOW
SS̄ ISOW (µm)
SS̄ DSOW (µm)
Years BP
Norm SS̄ DSOW
Norm SS̄ ISOW
Years BP
Norm SS̄ DSOW
Norm SS̄ ISOW